PAPER

Check for updates

Graphene oxide antagonizes the toxic response to arsenic *via* activation of protective autophagy and suppression of the arsenic-binding protein LEC-1 in *Caenorhabditis elegans*†

Hui Dai, [iD] [ab] Yun Liu,[a] Jingjing Wang, [iD] [ab] Yaguang Nie,[a] Yuxiang Sun,[a] Mudi Wang,[ab] Dayan Wang,[ab] Zhen Yang,[ab] Lei Cheng,[ab] Juan Wang,[ab] Jian Weng,[e] Qiuquan Wang, [iD] [d] Fangyue Wang,[f] Lijun Wu,[abc] Guoping Zhao[a] and An Xu*[abc]

Arsenic (As) pollution is a serious global problem and various technologies have been developed for As detoxification. Graphene oxide (GO) with its extraordinary structure and physicochemical properties has an excellent capability for the removal of As from contaminated water; however, the influence of GO on the toxic response to As(III), a well-established human carcinogen, is largely unknown. In the present study, *Caenorhabditis elegans* (*C. elegans*) was used as an *in vivo* model to clarify the role of GO at a non-toxic concentration in the toxic response to As(III) and its underlying molecular mechanisms. Our data showed that GO, irrespective of pretreatment or concurrent treatment with As(III), significantly blocked the toxic response to As(III). GO not only absorbed As(III), but also triggered protective autophagy, leading to efficient inhibition of oxidative stress, a major contributing factor in As(III) toxicity. Using laser ablation-inductively coupled plasma-mass spectrometry (LA-ICP-MS) and loss-of-function mutants, our data further showed that GO accelerated the excretion of As(III) from nematodes by suppressing the expression of As(III)-binding proteins LEC-1. Our data provided clear evidence that along with adsorption, the beneficial effects of GO in reducing As(III)-induced toxicity *in vivo* were mainly through protective autophagy coupled with downregulation of arsenic target protein expression, which might reveal new insights into the potential application of GO in water treatment and ecological risk assessment.

Environmental significance

Arsenic (As) pollution is a severe global problem nowadays. GO has been considered a promising nanomaterial for the removal of As in water treatment. We found that in addition to adsorption, GO reduced the toxicity of As(III) from two other aspects in living organisms. First, GO stimulated genuine autophagy to protect *C. elegans* from As(III)-induced oxidative stress and reproductive toxicity. Second, GO accelerated the excretion of As(III) by downregulating the expression of an As(III) binding protein LEC-1. Our data provide important information on a novel self-protection mechanism activated by nanomaterials in organisms to combat pollutant toxicity.

Introduction

Arsenic (As) is one of the most toxic metals derived from natural sources, mine effluents, and anthropogenic activities.[1]

The International Agency for Research on Cancer (IARC) has classified As and As compounds as carcinogenic agents to humans and they are associated with skin, lung, liver, urinary bladder, kidney, and colon cancers.[2] Millions of people

[a] *Key Laboratory of High Magnetic Field and Ion Beam Physical Biology, Chinese Academy of Sciences, Anhui Province Key Laboratory of Environmental Toxicology and Pollution Control Technology, Hefei Institutes of Physical Science, Anhui 230031, P. R. China*

[b] *University of Science and Technology of China, Hefei, Anhui 230026, P. R. China*

[c] *Institutes of Physical Science and Information Technology, Anhui University, Hefei, Anhui, 230601, P. R. China*

[d] *Department of Chemistry, College of Chemistry and Chemical Engineering, Xiamen University, Xiamen 361005, P. R. China*

[e] *Research Center of Biomedical Engineering, Department of Biomaterials, College of Materials, Xiamen University, Xiamen 361005, P. R. China*

[f] *Ore Deposit and Exploration Centre, School of Resources and Environmental Engineering, Hefei University of Technology, Hefei, 230009, P. R. China*

† Electronic supplementary information (ESI) available: Supporting figures showing the PCR primers for qRT-PCR; UV-vis absorption spectra of GO samples; average number of S-GO, I-GO, L-GO and As(III)-induced germline apoptotic cells; expression of autophagy related genes in wide type nematodes after exposure to 10 μg mL^{-1} S-GO, I-GO and L-GO for 24 h; expression of autophagy related genes in wild type and *lec-1(ok1597)* nematodes following 10 μg mL^{-1} L-GO treatment for 24 h. See DOI: 10.1039/c8en00244d

worldwide are chronically exposed to As at concentrations much higher than the guideline value (100 μg L^{-1} or greater) through contaminated drinking water, especially in West Bengal, Bangladesh, Thailand, Inner Mongolia, Taiwan, China, Mexico, Argentina, Chile, Finland, and Hungary.[3] The present available removal technologies for As include oxidation, phytoremediation, coagulation–flocculation, adsorption, ion exchange, electrokinetics and membrane technology.[4,5] However, these technologies have some drawbacks and their by-products can be potential sources for secondary As pollution. Therefore, there is an urgent need for developing low-cost, efficient, and environmentally friendly adsorbents for As removal and As detoxification *in vivo*.

Graphene oxide (GO) chemically exfoliated from oxidized graphite has been extensively explored as one of the most promising nanomaterials for application in environmental remediation and water purification.[6] GO consists of a layer with a π-conjugated structure of randomly distributed unoxidized aromatic regions and six-member aliphatic regions.[7] Abundant oxygenated functional groups, including hydroxyl (–OH), phenolic, epoxy (C–O–C), and carboxyl (–COOH), are available on the basal plane and sheet edges, which makes GO highly hydrophilic and stably dispersible in water. These extraordinary structural and physicochemical properties provide GO with an excellent capability to adsorb a broad range of organic and inorganic substances, such as small molecule drugs,[8] metal ions,[6,9] and organic compounds,[10] *via* hydrogen bonds and anion–π and electrostatic interactions. The positive charges on GO in acidic media showed high electrostatic interactions with inorganic As species.[11,12] Moreover, GO has proved to be a good candidate to support nanomaterial immobilization, which enables combined and synergistic actions that are highly desired for advance adsorption performance. A series of iron-decorated GO composites have been developed to significantly enhance As adsorption from contaminated water,[13–15] and these composites can be extracted rapidly by external magnetic fields without the need for filtration, centrifugation, and vacuum pumps.[11] Nanoparticles can adsorb biomolecules and travel to almost every location with organisms, the interactions between nanoparticles and organisms mediated by what adsorbs to the nanoparticle.[16–18] Considering that As is highly toxic and low doses of GO may be environmentally safe, a comprehensive assessment on the synergistic/antagonistic toxicity of GO and As should be carried out as an integral part of GO application in water purification. However, the influence of GO on the fate and transformation of and toxic response to As is largely unknown, and is of critical importance to understand its environmental and health impact.

Although the toxic effects of As(III) or GO alone have been well investigated both *in vitro* and *in vivo*, there is little available evidence to illustrate the combined effects of GO and As(III) and their underlying mechanisms are largely unknown. The phytotoxicity of As(v) in wheat was greatly amplified by GO, leading to a decrease in biomass and root number and increased oxidative stress.[19] GO at nontoxic concentrations increased the toxicity of As(III) by damaging the plasma membrane structure and fluidity in human hepatoma cells.[20] However, in contrast to these synergistic interactions, our previous study showed that GO pretreatment induced genuine autophagy in human–hamster hybrid cells, which inhibited the cytotoxicity and genotoxicity of polychlorinated biphenyls (PCBs).[21] These inconsistent observations may be a result of GO with different physicochemical properties, including surface area, layer number, lateral dimension, surface chemistry, and purity, the complicated interaction between GO and pollutants under different conditions, and the nature of the biological model system used. Therefore, it is necessary to evaluate the interaction between GO and As(III) and their toxic responses *in vivo*, which may provide essential information for better understanding the application of GO in purifying As(III)-contaminated water and the potential long-term health and ecological risks.

Among animal models, *Caenorhabditis elegans* (*C. elegans*) has emerged as a powerful genetic model in multiple fields of biomedical and environmental toxicology because of its tractable and fully sequenced genome, the availability of thousands of mutants, and its ability to manipulate genes and their expression through transgenic approaches and RNAi techniques.[22–24] As a nematode, *C. elegans* represents organisms that are ubiquitously present in the ecosystem and has been well-documented in the investigation of the toxicity and toxicological mechanisms of various heavy metals and nanoparticles.[25,26] Trivalent arsenic (As(III)) and pentavalent arsenic (As(v)) are the two main valence states of As in nature. As(III) has been reported to be more mobile and approximately 60 times more toxic than As(v).[27] Using *C. elegans* as an *in vivo* assay system, the present study focused on clarifying the protective role of GO in decreasing As(III)-induced toxicity and the underlying molecular mechanisms. To determine the influence of GO on As(III) toxicity, the nematodes were exposed to GO and As(III) in different ways. The presence of GO irrespective of pretreatment or concurrent treatment with As(III) significantly blocked the toxic response to As(III). In addition to adsorption, GO stimulated genuine autophagy to protect *C. elegans* from As(III)-induced oxidative stress and reproductive toxicity. Moreover, GO suppressed the expression of the As(III)-binding protein LEC-1 and accelerated the clearance of As(III) accumulated in *C. elegans*. Our data provide basic information on a novel self-protection mechanism activated by nanomaterials in organisms to combat pollutant toxicity.

Materials and methods

Preparation of GO and characterization of the physicochemical interaction between GO and As(III)

GO materials were synthesized from graphite by the modified Hummers method.[28] Briefly, graphite (2 g, purchased from Qingdao BCSM. Co., Ltd. China) and sodium nitrate (1 g)

1712 | *Environ. Sci.: Nano*, 2018, **5**, 1711–1728

This journal is © The Royal Society of Chemistry 2018

were dispersed in H_2SO_4 (50 mL) in ice and $KMnO_4$ (7 g) was further added. After oxidation, the samples were washed, filtered, and centrifuged three times. Thereafter, the dry GO powder was collected by freeze-drying. The concentration of the GO solution was adjusted to 1 mg mL^{-1} with sterile water, followed by placing it in a bath sonicator for 4 h with a 100 Hz, 200 W ultrasonic cleaner (KunShan, JiangSu, China), with water changed every hour. The samples were then centrifuged for 30 min at $2000 \times g$ (multispeed centrifugation, Thermo, CL31R, Waltham, MA, USA) and the supernatant was collected. This procedure was repeated twice. The prepared GO samples were named as larger-sized GO samples (L-GO). Afterward, L-GO was used as a substrate for preparing intermediate-sized GO (I-GO) and smaller-sized GO (S-GO) particles. I-GO and S-GO were prepared through probe sonication (ultrasonic cell disrupter, Sciencent Z. JY G2-HNNingbo, China) with cycles of 15 s work and 15 s rest at an ultrasonic power of 65 w in ice for 10 min (I-GO) and 30 min (S-GO). For GO mass quantification, the gradient dilution method was used to prepare a standard curve by ultraviolet spectrophotometry (Shimadzu, UV-3600, Kyoto, Japan).

Atomic force microscopy (AFM) samples were prepared by depositing the dispersion on mica substrates and then dried at room temperature, using a DI MultiMode V scanning probe microscope (MultiMode V, Bruker). Transmission electron microscopy (TEM) analysis of GO was performed using an H-7650 transmission electron microscope (Hitachi Scientific Instruments, Japan). The TEM samples were prepared by depositing a small drop of the solution onto a carbon-coated copper electron microscopy grid. The surface charge of the samples, either suspended in Milli-Q water (Millipore, 18 MΩ cm) or in K-medium (32 mM KCl and 51 mM NaCl), was analyzed using a Zetasizer (Malvern Nano series, Malvern, U.K.). A Raman spectrometer (Renishaw, UK) with a 514 nm laser was employed to analyze the structure of GO. The FTIR spectra of the GO materials were recorded on a Nicolet 6700 FTIR spectrophotometer (Thermo Fisher Scientific Inc., USA) using the KBr pellet method. The GO samples were deposited onto silicon wafers and air-dried, and the silicon wafers were then subjected to X-ray photoelectron spectroscopy.

The morphology of GO or the mixture of GO and As(III) in Milli-Q water was determined by TEM to evaluate the morphological changes. The selected area electron diffraction (SAED, JEOL 2100 HT, JEOL, Tokyo, Japan) pattern revealed the disordered nature of GO. An energy dispersive X-ray spectrometer (EDX JEOL, 2100 HT, JEOL, Tokyo, Japan) was used for the qualitative analysis of elements on the surface of GO samples.

C. elegans strains and maintenance

All worm strains were maintained on nematode growth medium (NGM) plates seeded with *Escherichia coli* (*E. coli*) OP50 at 20 °C, according to standard protocols.[29] The wild type strain used was Bristol N2. The following strains were provided by the *Caenorhabditis elegans* Genetics Centre (CGC): N2, *rpl-43 (bp399)*, *mev-1*(*kn 1*) and *lec-1*(*ok1597*).

Preparation of GO dispersion and As(III) solution and worm exposure

GO samples were suspended in Milli-Q water to obtain a stock solution of 1.0 g L^{-1} and were then briefly sonicated (40 kHz) for 20 min before use. We obtained sodium arsenite ($NaAsO_2$, hereafter simply referred to as As(III); 99.5% purity; GR, 100041) from Chengdu Aikeda Chemical Reagent Co., Ltd., Chengdu, China) to prepare the As(III) stock solutions and stored the stock solutions in the dark at 4 °C until usage. Different working concentrations were prepared by diluting the stock solutions with K-medium. The worms were cultured for 48 h, which were then treated singly or co-treated with varying concentrations of GO (10 µg mL^{-1}) or As(III) (1, 5, and 10 µM) and incubated for 24 h. For adsorption experiments, we prepared all exposure media 24 h prior to use to allow the adsorption of As(III) on GO to reach equilibrium.

Toxicity assays

The toxicity was assessed by means of the endpoints of germline apoptosis, the brood size, and the number of oocytes. Apoptotic germ cells were measured using Acridine orange (AO, Molecular Probes, Eugene, OR) vital staining as described previously.[30] Briefly, synchronized worms at the L4 stage of development were exposed to graded concentrations of working solutions for 24 h; adult worms were then placed into 200 µL of 75 µg mL^{-1} AO and OP50. After 60 min of incubation at 20 °C, worms were allowed to recover for 60 min on an NGM plate to clear the excess AO from their intestines. The worms were then immobilized using sodium azide (NaN_3) and fluorescent staining was observed under an Olympus IX71 microscope (Olympus, Tokyo, Japan). The apoptotic cells appeared yellow-green after AO staining, representing increased DNA fragmentation, whereas intact cells were uniformly green. The brood size was determined by placing single worms onto individual plates, the P0 nematode transferred to a new plate everyday. The number of hatched progeny was counted the day following transfer.[31] The oocytes were mounted onto agar pads on microscope slides in 5 M NaN_3 in M9 buffer, after which the number of oocytes located from the spermatheca to the gonad loop per gonad arm of a nematode was counted under an optical microscope.

As(III) accumulation and mapping in C. elegans

An inductively coupled plasma atomic fluorescence spectrometer (ICP-AFS) was used to monitor the cellular As(III) content. The worms were exposed to graded doses of As(III) or co-exposed to graded doses of GO and As(III) for 24 h. After treatment, 5 mg of dry worms were placed in an Erlenmeyer flask, and 5 mL 75% HNO_3 was added. After predigestion at room temperature for approximately 12 h, the flask was heated at

This journal is © The Royal Society of Chemistry 2018

Environ. Sci.: Nano, 2018, **5**, 1711–1728 | **1713**

150 °C on an electric hot stainless-steel plate, until the solution changed from chartreuse to clear. All digestive solutions were quantitatively transferred to 5 mL polypropylene centrifuge tubes with Milli-Q water, and brought to a final volume. These were then subjected to ICP-AFS (Optima 7300 DV) for total As(III) detection.

LA-ICP-MS was applied to study the uptake and accumulation of As(III) in *C. elegans*. The L4 worms were washed after incubation and suspended in Milli-Q water. This solution was dropped onto microscopic slides and the collected worms oven-dried at 60 °C overnight in order to obtain single, separated worms at a constant weight.[32,33] Bioimaging tests were performed at the Ore Deposit and Exploration Centre (ODEC), using a laser ablation system (Photon Machines Analyte HE with a 193 nm ArF Excimer), coupled to a quadrupole-based inductively coupled plasma-mass spectrometer (ICP-MS) (Agilent 7900). Analyte HE utilizes a two-volume ablation cell designed by Laurin Technic Pty. Ablation was performed in an atmosphere of UHP He (0.9 min^{-1}), and upon exiting the cell the aerosol was mixed with Ar (0.87 l min^{-1}) immediately after the ablation cell *via* a T-connector before entering the ICP. The ICP-MS system was optimized daily to maximize the sensitivity to isotopes of the mass range of interest, while maintaining the lowest possible production of molecular oxide species (*i.e.*, 232Th16O/232Th), usually <0.2%. Elemental maps were created by ablating sets of parallel line rasters in a grid across the sample. A beam size of 8 μm and a scan speed of 8 μm s^{-1} were chosen in this study. A laser repetition of 10 Hz was selected at a constant energy output of 80 mJ, resulting in an energy density of ~2 J cm^{-2} at the target. A 20 s background acquisition was acquired at the beginning of scanning, and a delay of 20 s was used after ablation to allow for cell wash-out, gas stabilization, and computer processing. Reference materials (NIST-610 or GSE-1G) at the start and end of each mapping were analyzed for data calibration. Images were compiled and processed using the program LaIcpMsSoftWare2.2 (in-house designed mapping reduction software based on MATLAB). For each raster and every element, the average background was subtracted from its corresponding raster, and the rasters were compiled into a 2-D image displaying the combined background/drift corrected intensity for each element.

Reverse-transcription and quantitative real-time polymerase chain reaction (qRT-PCR) assay

Total RNA was extracted and reverse-transcribed using a Takara RNA Kit (Takara Bio., Japan). After cDNA synthesis, RT-PCR was performed using an SYBR Green qPCR mix (Applied Biosystems, USA) on an ABI Step-one Plus RT-PCR system (Applied Biosystems). The final results were expressed as the relative expression ratio between the targeted gene and the reference *act-1* gene. All reactions were performed in triplicate. The primers used for the PCR reactions are listed in ESI† Table S1.

RNA interference (RNAi)

RNAi was carried out following standard procedures.[34] Briefly, bacteria expressing doubled-stranded RNA to a specific worm gene were grown on NGM plates containing 25 μg mL^{-1} carbenicillin and isopropyl 1-thio-β-D-galactopyranoside (IPTG, 1 mM). Larvae at the L1 stage of development were placed on the RNAi-feeding bacterial plates and allowed to develop to the L4 stage. The empty vector L4440 was used as the negative control in all RNAi experiments, and a *unc-15* RNAi clone was included in the experiments as the positive control.

Mitochondrial membrane potential assay

The fluorescent probe JC-1 (purchased from Sigma-Aldrich, Shanghai, China) was used to determine the mitochondrial membrane potential as described.[35] JC-1 was dissolved in DMSO and then added to M9 buffer containing young adult worms. The worms were incubated with the dye for 2 h at 20 °C and then transferred to NGM plates. The stained worms were paralyzed using levamisole (Sigma) and observed under an LSM 710 laser scanning confocal microscope (Carl Zeiss, Inc., Germany). The intensity of red- or green-channel fluorescence for mitochondria was measured using Zen 2010 light edition (Carl Zeiss, Inc., Germany), and the red : green ratio was calculated. At least 20 worms were viewed for each treatment and three replicates were performed.

Reactive oxygen species (ROS) detection

The ROS assay was performed using 5′,6′-chloromethyl-2′,7′-dichlorodihydro-fluorescein diacetate (CM-H$_2$DCFDA, Sigma-Aldrich, Shanghai, China), based on a previously described method.[36] After exposure, the worms were transferred to M9 buffer containing 1 μM CM-H$_2$DCFDA, incubated for 2 h at 20 °C in the dark without addition of food and were viewed by laser scanning confocal microscopy at a 488 nm excitation wavelength and with a 517–530 nm emission filter (Carl Zeiss, Inc., Germany). The relative fluorescence intensity of the intestine was semi-quantified, expressed as relative fluorescence units (RFU). At least 20 worms were viewed for each treatment and three replicates were performed.
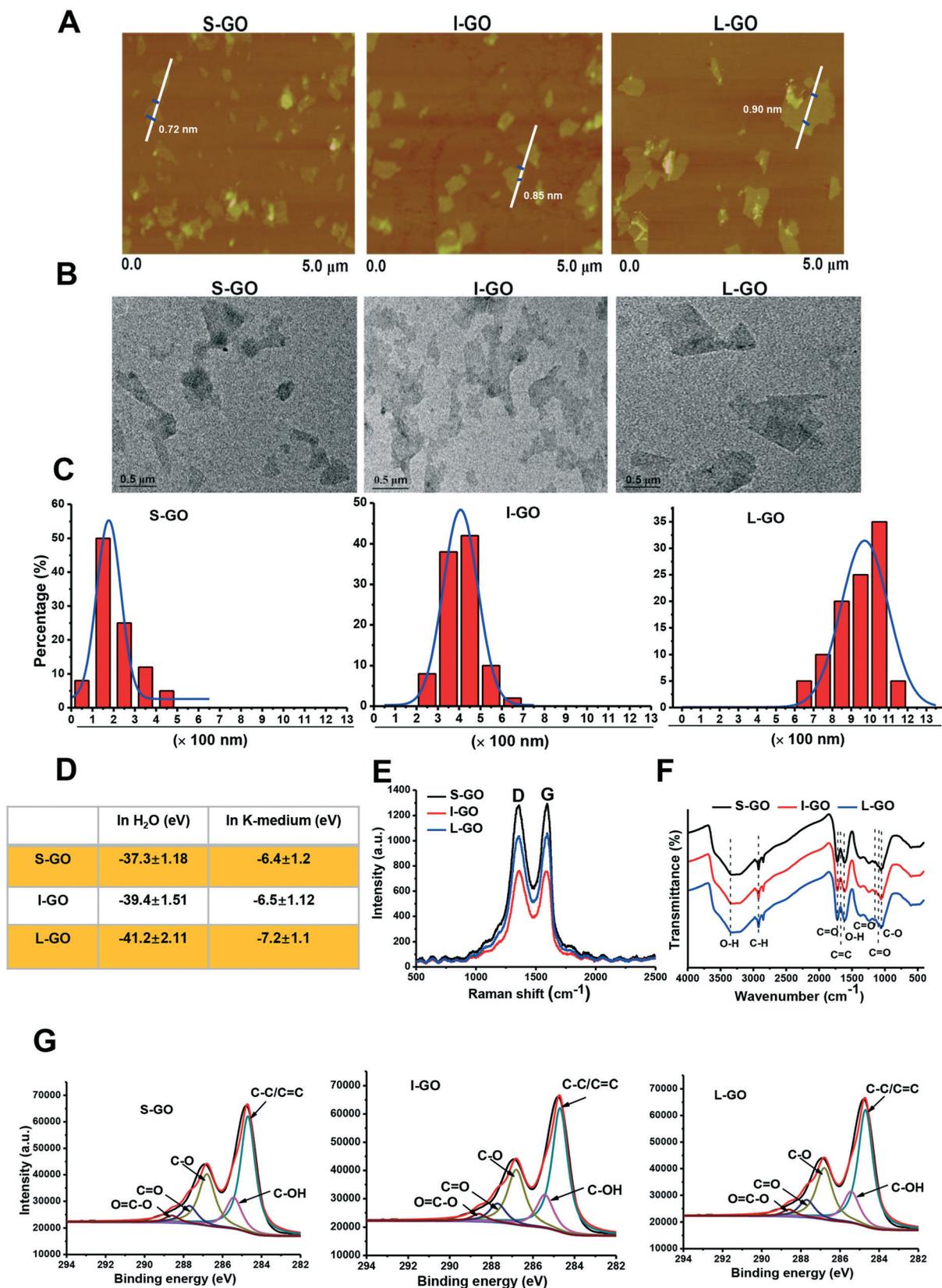
Statistical analysis

All treatments included three replicates. All data are shown as the mean ± standard deviation and were analyzed by *t*-test and one-way analysis of variance (ANOVA). $P < 0.05$ was considered statistically significant. The relative fluorescence from the fluorescence images was determined metrically using Image-Pro Plus, version 6.0.

Results

Physicochemical characterization of GO with various sizes

The morphology of GO samples with different lateral sizes was visualized by AFM. As shown in Fig. 1A, the average

1714 | *Environ. Sci.: Nano*, 2018, **5**, 1711–1728

This journal is © The Royal Society of Chemistry 2018

Fig. 1 Characterization of GO samples. (A) Representative AFM topography of S-GO, I-GO, and L-GO. (B) Representative TEM images of S-GO, I-GO, and L-GO. (C) Histogram of GO size distribution developed by counting 100 sheets for each sample, with Gaussian fit curves in each histogram. (D) Zeta potential of S-GO, I-GO, and L-GO in Milli-Q water and K-medium (n = 3). (E) Raman spectra and curve fitting of D and G bands. (F) Identification of functional groups on the GO surface using FTIR spectroscopy (range: 4000–400 cm^{-1}). (G) Characterization of the surface composition of GO samples using XPS.

This journal is © The Royal Society of Chemistry 2018

Environ. Sci.: Nano, 2018, **5**, 1711–1728 | **1715**

thickness was approximately 1.0 nm in topographic height for all samples, suggesting that they were composed of single-layered graphene sheets.[37] The difference in lateral size among the GO samples was confirmed by TEM (Fig. 1B). Size distribution analysis showed that most GO sheets ranged from 50–350 nm for S-GO (smallest), from 250–850 nm for I-GO (intermediate), and from 650–1050 nm for L-GO (largest) (Fig. 1C). To ensure that the sample preparation processes did not alter physicochemical properties other than lateral size, we performed detailed physiochemical characterization for these GO samples. Surface charge was analyzed by zeta-potential assessment. As shown in Fig. 1D, these GO samples were similarly negatively charged when suspended either in Milli-Q water or in K-medium. The ultraviolet-visible (UV-vis) spectra showed an adsorption peak at 227 nm for all these samples (Fig. S1†), which was similar to the reported feature in the range of 227–231 nm for GO.[38] Furthermore, upon Raman spectrometry with a 514 nm laser employed to

analyze the structure of GO, the D peak at 1348 cm^{-1} and the G peak at 1599 cm^{-1} representing the two typical peaks of GO were observed for all GO sheets (Fig. 1E). Additionally, Fourier transform infrared (FTIR) spectroscopy was employed for identifying the presence of functional groups on the surface of GO sheets. The spectrum was obtained from 4000 to 400 cm^{-1} using FTIR, and the peaks at 3352 cm^{-1} and 1627 cm^{-1} were attributed to residual O–H stretching vibration, whereas bands denoting C–O and C=O stretching of the COOH group were located at 1034 cm^{-1} and 1150 cm^{-1}. Meanwhile, the C=O vibration band was identified at 1160 cm^{-1}, and the band corresponding to the C=O stretching vibration of COOH was located at 1710 cm^{-1}. Furthermore, bands representative of C–H stretching were recognized at 3000–2900 cm^{-1} (Fig. 1F). In Fig. 1G, X-ray photoelectron spectroscopy (XPS) displayed similar profiles for all GO sheets, with characteristic peaks at 284.8, 286, 286.5, and 288.8 eV, representing the C–C/C=C, C–OH, C=O, and O=C–OH
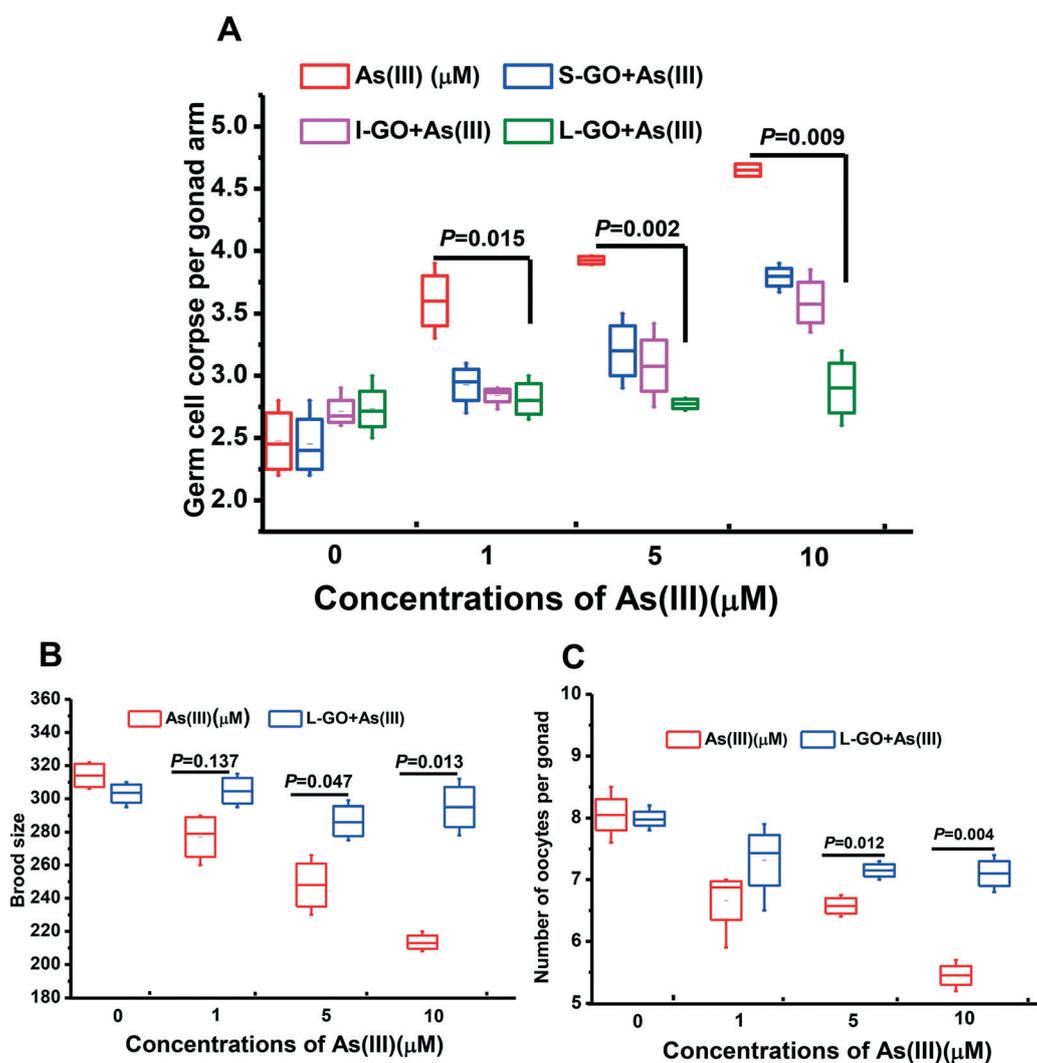

Fig. 2 Combined toxicity of GO and As(III). (A) Three GO samples (10 μg mL^{-1}) with distinct lateral sizes of particles were incubated with As(III) (1, 5, and 10 μM) for 24 h, and then the worms were treated with the mixture for another 24 h. Effect of co-exposure to L-GO and As(III) on the (B) total brood size and (C) oocytes of worms. Results are means ± S.D. of triplicate values (n = 3) from three experiments.

1716 | Environ. Sci.: Nano, 2018, 5, 1711–1728

This journal is © The Royal Society of Chemistry 2018

groups, respectively. Taken together, these characterization data revealed that S-GO, I-GO, and L-GO samples showed comparable physicochemical properties except for lateral size differences.

Effect of lateral size on As(III) toxicity with or without GO

As shown in Fig. S2A,† S-GO, I-GO, and L-GO at concentrations ranging from 0 to 10 µg mL^{-1} essentially had no effect on germline apoptosis in *C. elegans*. In contrast, a concentration-dependent increase in germline apoptosis at the meiotic zone of the gonad of *C. elegans* exposed to As(III) was observed. A significant increase in germline apoptosis over the background level was observed in *C. elegans* exposed to As(III) at concentrations ≥1 µM ($P < 0.05$) (Fig. S2B†). In the present study, the non-toxic concentration of GO, 10 µg mL^{-1}, was used to eliminate its toxic effect on *C. elegans* concurrently exposed to As(III).

To investigate the influence of GO on As(III) toxicity, S-GO, I-GO, and L-GO were incubated with As(III) (1 µM, 5 µM, and 10 µM) for 24 h *in vitro*, and the nematodes were then exposed to the mixture of GO and As(III) for another 24 h. As shown in Fig. 2A, germline apoptosis was increased from the background level of 2.55 ± 0.14 to 3.6± 0.19, 3.92± 0.02, and

4.65 ± 0.08 when the As(III) concentrations were 1 µM, 5 µM, and 10 µM, respectively. However, the germline apoptosis induced by As(III) at the concentrations of 1 µM, 5 µM, and 10 µM could be reduced by the presence of S-GO, I-GO, and L-GO. In particular, L-GO at 10 µg mL^{-1} significantly inhibited germline apoptosis from 3.6 ± 0.19 to 2.765 ± 0.09, 3.92 ± 0.02 to 2.795 ± 0.008, and 4.65 ± 0.08 to 2.865 ± 0.21 at As(III) concentrations of 1 µM, 5 µM, and 10 µM, respectively ($P < 0.05$).

To confirm these observations, the brood size and number of oocytes per gonad, which are two essential indicators for reproductive toxicity, were determined in *C. elegans* concurrently exposed to L-GO and As(III). As shown in Fig. 2B and C, the presence of L-GO could dramatically increase the brood size and the number of oocytes in *C. elegans* exposed to As(III) (1 µM, 5 µM, and 10 µM). These results indicated that concurrent exposure of L-GO with As(III) could dramatically decrease the reproductive toxicity of As(III) in *C. elegans*.

Physicochemical interaction between GO and As(III) and toxicity of adsorbed As(III)

As shown in Fig. 3A, As(III) had a slight influence on the morphology of L-GO as observed by TEM, whereas the SAED
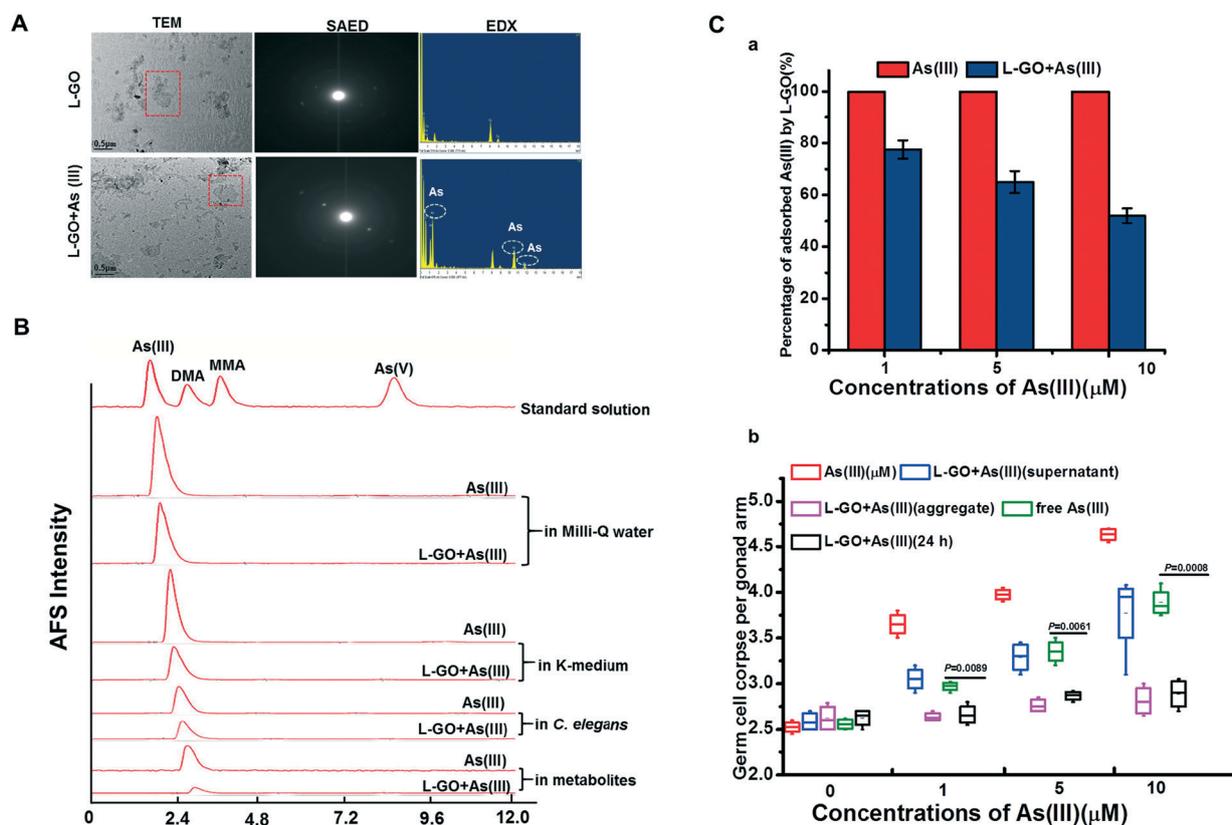
Fig. 3 Interaction between L-GO and As(III) and toxicity of adsorbed As(III) and free As(III). (A) Low-resolution TEM image with corresponding SAED patterns (red squares) and EDX spectroscopy image of L-GO with or without As(III) in Milli-Q water. (B) Chromatograms of As(III), dimethylarsinic acid (DMA), monomethylarsonic acid (MMA), As(v) standard solution (80 ng mL^{-1}), and As(III) in the absence or presence of GO in Milli-Q water, K-medium, worms, and metabolites. (C) ICP-AFS analysis to quantitatively determine As(III) adsorbed on L-GO and the toxicity of the supernatant, aggregate, and equivalent free As(III) in the supernatant of the L-GO and As(III) mixture, and L-GO and As(III) co-exposure.

This journal is © The Royal Society of Chemistry 2018

Environ. Sci.: Nano, 2018, **5**, 1711–1728 | **1717**

patterns showed that the clear diffraction dots of L-GO disappeared in the presence of As(III), indicating that As(III) also altered the crystal structure of L-GO. EDX showed the presence of As(III) element on L-GO, whereas no As(III) peaks were observed in the L-GO-free regions. High-performance liquid chromatography-inductive coupled atomic fluorescence spectrometry (HPLC-AFS) analysis revealed no chemical form changes of As(III) in the presence of GO, irrespective of examination in K-medium, nematodes and the metabolites exposed to As(III) (Fig. 3B).

To determine the toxicity of As(III) adsorbed on GO and the As(III) residue in the medium, L-GO at 10 μg mL^{-1} was incubated with 1 μM, 5 μM, and 10 μM As(III) for 24 h and the mixture was then centrifuged at 24 000 rpm. As shown in Fig. 3C-a, the amount of elemental As(III) in the supernatant with As(III) treatment alone was 100%, which was decreased significantly by 77.5% ± 3.53%, 65% ± 4.24% and 52% ± 2.83% (for As(III) 1, 5, and 10 μM, respectively) in the presence of L-GO. Germline apoptosis induced by As(III) in the supernatant was reduced, when *C. elegans* was exposed to As(III) (1, 5, and 10 μM, respectively) concurrently with L-GO (Fig. 3C-b). The GO–As(III) aggregates in the sediment had no effect on the induction of germline apoptosis; in contrast, the germline apoptosis induced by free As(III) in the supernatant was similar to As(III) treatment alone at equivalent concentrations. These data indicated that in addition to adsorption, other mechanisms might be involved in the L-GO mediated decrease in As(III) toxicity in *C. elegans*.

Effect of exposure manner on As(III) toxicity with or without GO

To further explore the influence of GO exposure manner on As(III) toxicity, *C. elegans* was exposed to As(III) in the presence or absence of L-GO in two other different methods. In the first method, the nematodes were pretreated with GO for 12 h, and then graded concentrations of As(III) were added into the medium for a further 12 h. In the second process, the nematodes were pretreated with graded concentrations of As(III) for 12 h, and GO was then added into the medium for a further 12 h. L-GO pretreatment could decrease the germline apoptosis induced by As(III) to near background levels which was similar to the observation in worms concurrently exposed to GO and As(III). In contrast, L-GO had a minimal effect on the As(III) toxicity in *C. elegans* that were pretreated with As(III) (3.3 ± 0.2, 4.065 ± 0.13, and 4.23 ± 0.19, respectively) (Fig. 4). These results indicated that it was necessary for GO to interact with the nematodes to decrease the toxicity of As(III) *in vivo*. Thus, we hypothesized that a protective mechanism may be stimulated by the presence of GO.

Effect of GO on mitochondrial dysfunction induced by As(III)

Mitochondria are an important target in the toxic response to As(III) *in vivo*. As shown in Fig. 5A, the mitochondria of untreated nematodes exhibited a normal morphology, with an oval shape and an intact structure. In As(III)-exposed nematodes, the mitochondria exhibited an abnormal appearance such as swelling, deformation, ruptured double membrane, reduction or vanishing of the crista, and vacuolation; however, the presence of L-GO rescued the mitochondrial damage induced by As(III).

To ascertain the effect of L-GO on the mitochondria dysfunction induced by As(III), the mitochondrial membrane potential was determined using the 5,5′,6,6′-tetrachloro-1,1′,3,3′-tetraethyl benzimidalyl carbocyanide iodide (JC-1) stain in worms exposed to As(III) with or without L-GO. In worms with a normal mitochondrial function, J-aggregates with intense red fluorescence formed in highly polarized mitochondrial membranes, as shown in unexposed worms (Fig. 5B-1). As(III) treatment resulted in more JC-1 in the green fluorescent monomeric form, whereas more red fluorescence was retained in worms co-exposed to As(III) and L-GO. Quantification of the ratio of red to green fluorescence showed that As(III) dramatically suppressed the mitochondrial membrane potential, which was blocked by L-GO (Fig. 5B-2).

Using a fluorescent probe specific for ROS, a significant increase in fluorescence intensity over the background level was observed in nematodes exposed to As(III) (Fig. 5C-1), indicating that As(III) stimulated oxidative stress *in vivo*. The relative fluorescence intensity induced by As(III) decreased from 477.5 ± 21.6 to 195.2 ± 8.8 in the presence of L-GO ($P < 0.05$) (Fig. 5C-2). L-GO alone at a concentration of 10 μg mL^{-1} had a minimal effect on ROS induction.

In *C. elegans*, *mev-1* encodes cytochrome b, an integral membrane protein that is a subunit of mitochondrial respiratory chain complex II (ubiquinol-cytochrome c reductase).[39] The spontaneous germ cell apoptosis in *mev-1(kn 1)* mutants was found to be 3.55 ± 0.14, which was higher than that in wild type nematodes (2.55 ± 0.21). L-GO does not suppress the increased germ cell apoptosis in *mev-1(kn 1)* mutants; the germ cell apoptosis induced by As(III) in *mev-1(kn 1)* mutants
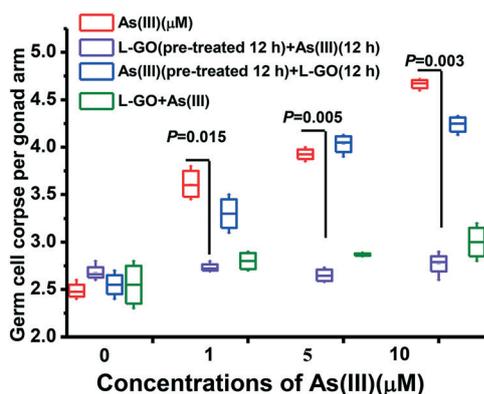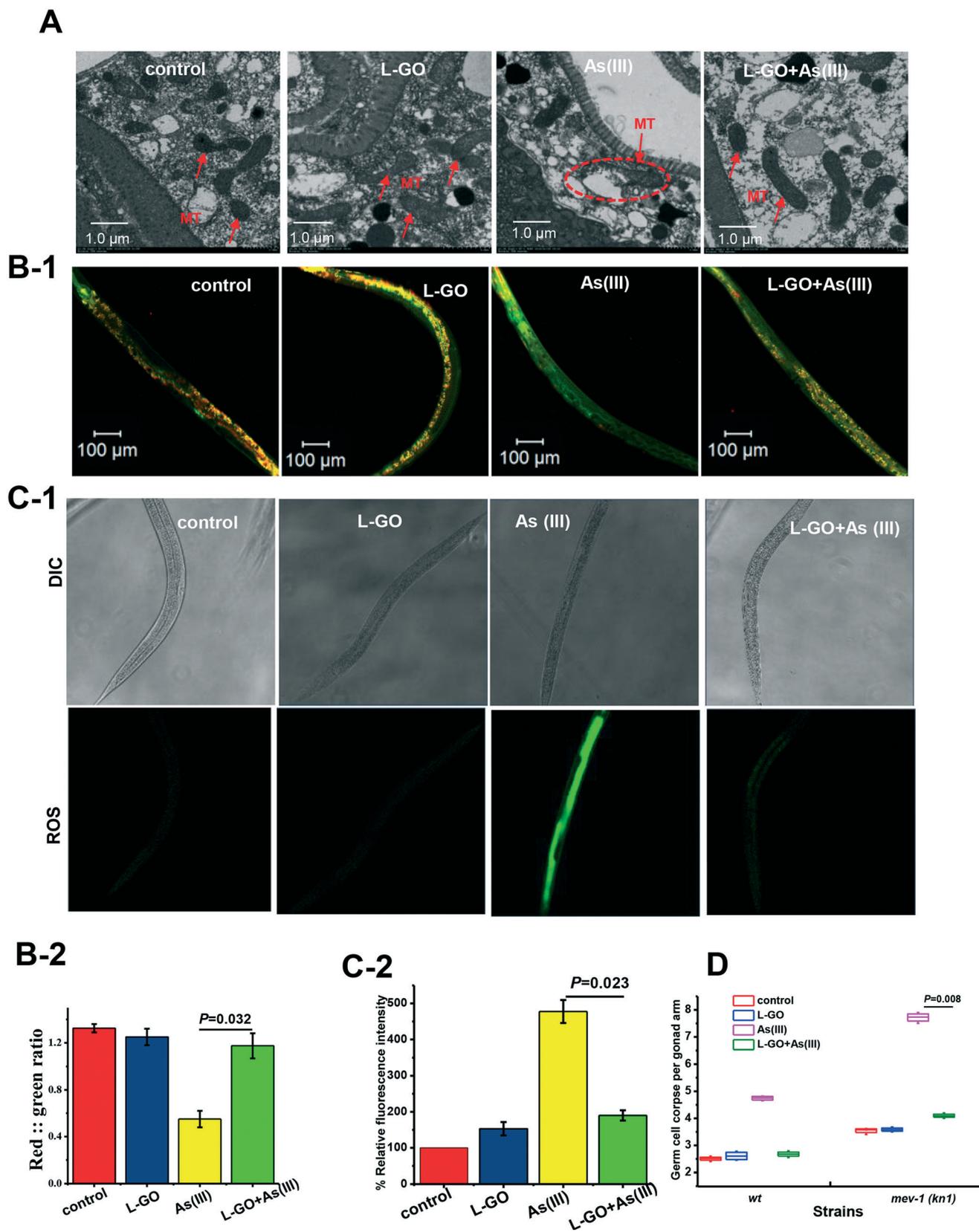

Fig. 4 Effect of exposure manner on As(III) toxicity with or without GO. Worms were pretreated with As(III) (1, 5, and 10 μM) for 12 h, followed by exposure to L-GO (10 μg mL^{-1}) for another 12 h, and worms were pretreated with L-GO (10 μg mL^{-1}) for 12 h, followed by exposure to As(III) (1, 5, and 10 μM) for another 12 h. Results are means ± S.D. of triplicate values (n = 3) from three experiments.

1718 | *Environ. Sci.: Nano*, 2018, **5**, 1711–1728

This journal is © The Royal Society of Chemistry 2018

Fig. 5 Oxidative stress response to K-medium, L-GO, As(III) and concurrent exposure to L-GO and As(III). (A) TEM images of *C. elegans* after exposure to K-medium, L-GO, As(III), or both. Red arrows indicate mitochondria. (B) Mitochondrial membrane potential indicated by JC-1 specific fluorescence; worms were treated with K-medium, L-GO, As(III), or both. (C) The global ROS production was quantified using CM-H$_2$DCFDA. (D) Average number of germline apoptotic cells induced by exposure to K-medium, L-GO, As(III) or both in wild type and mutant *mev-1(kn 1)* strains. Results are means ± S.D. of triplicate values (*n* = 3) from three representative experiments.

This journal is © The Royal Society of Chemistry 2018

Environ. Sci.: Nano, 2018, **5**, 1711–1728 | **1719**

was significantly higher than that in wild type nematodes at equal concentrations, indicating that the *mev-1(kn 1)* mutant are hypersensitive to As(III) exposure. Similarly, the germ cell apoptosis induced by As(III) was significantly suppressed from 7.6 ± 0.35 to 4.25 ± 0.15 with co-exposure to As(III) and L-GO (Fig. 5D). These results indicated that L-GO protected *C. elegans* from reproductive toxicity induced by As(III) by reducing the mitochondrial dysfunction.

GO decreased the toxicity of As(III) *via* the activation of autophagy

Autophagy as an evolutionarily conserved intracellular catabolic process for the degradation of endogenous or foreign contents in the cytoplasm has been implicated in a variety of toxicity response and pathological processes.[40] Under TEM, formation of autophagic vacuoles with a double membrane and engulfment were observed in worms exposed to L-GO alone and to concurrent treatment with L-GO and As(III) (Fig. 6A). *lgg-1*, *bec-1*, *unc-51*, and *atg-7* are essential genes for the autophagy process.[41] qRT-PCR analysis revealed that the mRNA level of *bec-1*, *lgg-1*, *unc-51* and *atg-7* in nematodes exposed to L-GO was significantly upregulated 4.65 ± 0.14, 3.45 ± 0.21, 4.55 ± 0.49 and 3.65 ± 0.17-fold, respectively, as compared to control nematodes. Although the transcription of *bec-1*, *lgg-1* and *unc-51* was not upregulated in worms exposed to As(III) alone at 10 μM, the presence of L-GO significantly increased the mRNA level of these three genes in nematodes exposed to As(III) (Fig. 6B). By partial RNAi targeting of three different autophagy genes, we further found that L-GO had a significantly lower effect on As(III) toxicity in nematodes subjected to *bec-1*, *lgg-1* and *atg-7* RNAi compared to wild type worms (Fig. 6C).

Using 3-methyladenine (3-MA), a widely used inhibitor of autophagy,[42,43] we further investigated the role of autophagy in As(III)-induced germline apoptosis in nematodes concurrently exposed to L-GO. As shown in Fig. 6D, L-GO evidently suppressed the germline apoptosis induced by As(III) (10 μM) from 3.875 ± 0.21 to 2.75 ± 0.09. In the presence of 3-MA, the germline apoptosis in worms co-exposed to L-GO and As(III) showed no significant changes compared to As(III) treatment alone. Moreover, 3-MA alone at the same concentrations showed no effect on germline apoptosis. Autophagy is a dynamic flux, and its downstream degradation is essential for maintaining its protective role in intracellular homeostasis. Bafilomycin A1 (BFA), which inhibits vacuolar H$^+$-ATPase and prevents fusion between autophagosomes and lysosomes, was employed to detect the integrity of the autophagy flux.[44] As shown in Fig. 6E, no significant difference in the level of apoptosis was observed in nematodes co-exposed to L-GO and As(III) in the presence of BFA, compared to As(III) treatment alone with BFA. These data indicated that the As(III)-induced toxic response was ameliorated by L-GO mediated autophagy in *C. elegans*.

To verify that L-GO elevated the autophagic activity, transgenic strains harboring *rpl-43(bp399);bpIs151[Psqst-1::SQST-1::GFP]* were used for observing autophagy induction using confocal microscopy. SQST-1::GFP as an autophagy substrate

is constantly produced and degraded by autophagy, thus maintaining a very low level in intestinal cells under normal conditions.[45] In *rpl-43 (bp399)* hypomorphic mutants, the autophagy substrate SQST-1::GFP is not degraded by autophagy and shows aggregated signals in the intestinal cells. As shown in Fig. 6F, nematodes exposed to L-GO alone or co-exposed to L-GO and As(III) showed significantly less intestinal SQST-1::GFP aggregation compared to worms exposed to As(III) alone ($P < 0.05$), indicating the activation of autophagy by L-GO in the presence or absence of As(III) in *C. elegans*. These results provide *in vivo* evidence that the autophagy flux activated by L-GO is involved in cellular defense against As(III)-induced toxicity.
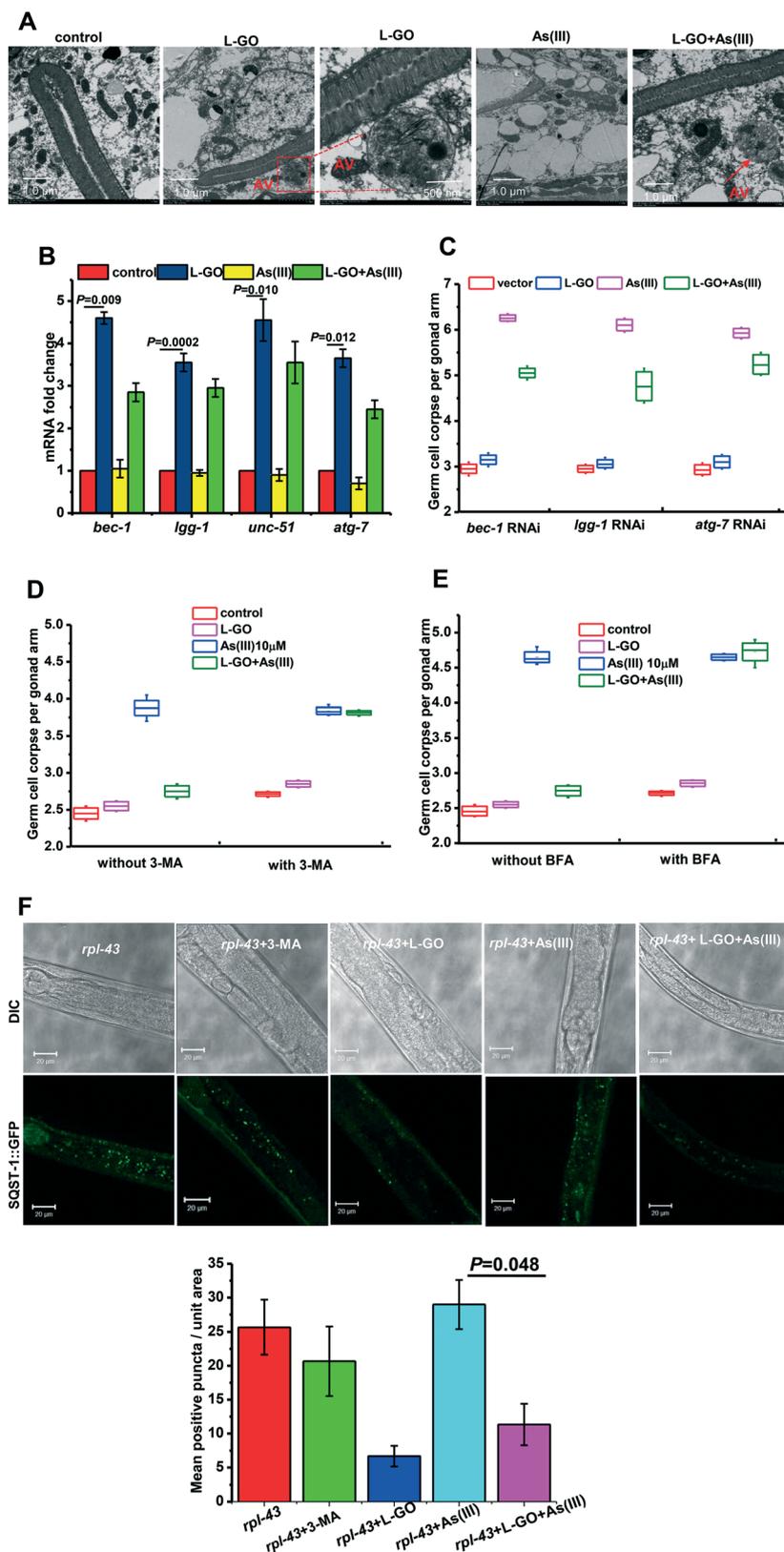
Autophagy induced by GO blocked the ROS production

Oxidative stress plays an important role in As(III) toxicity. The effect of autophagy induced by L-GO on ROS generation was determined in nematodes exposed to L-GO alone, As(III) alone, and L-GO concurrently treated with As(III), respectively. As shown in Fig. 7A-1 and A-2, there was no significant induction of ROS production in *bec-1* RNAi treated nematodes exposed to L-GO. In contrast, a significant increase in ROS was observed in *bec-1* RNAi treated nematodes, exposed to As(III) alone or co-exposed to L-GO and As(III). By itself, 3-MA had no effect on ROS generation. However, L-GO had no effect on As(III) induced ROS in the presence of 3-MA (Fig. 7B-1 and B-2). These data suggested that autophagy activated by L-GO inhibited the generation of As(III)-induced ROS in worms.
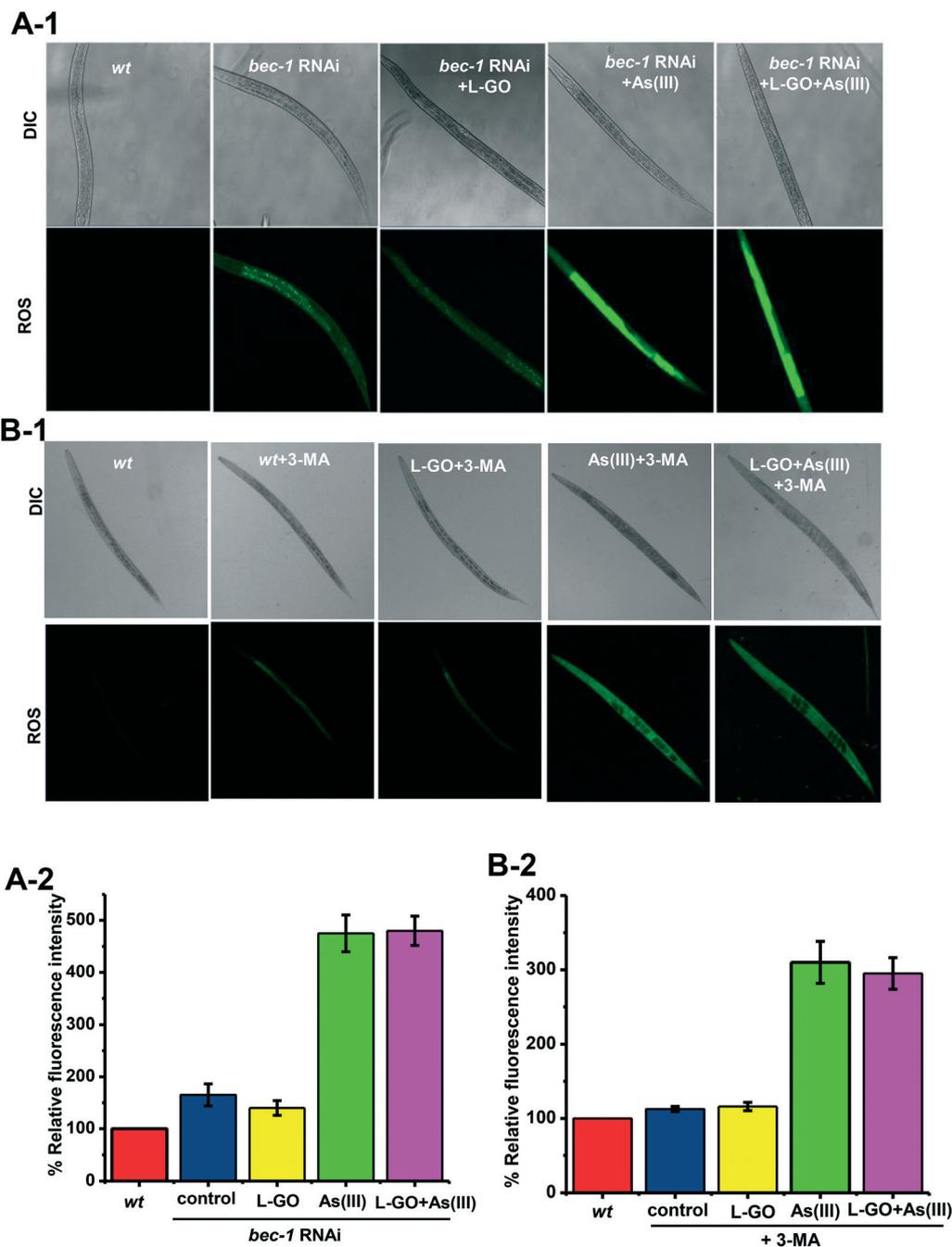
GO accelerated As(III) clearance by suppressing the gene expression of As(III)-binding protein (LEC-1)

LEC-1 is homologous to vertebrate Galectin-1 (GAL1), which serves as a target protein of As(III) *in vivo*. L-GO dramatically suppressed the expression of *lec-1* in wild-type nematodes, as shown in Fig. 8A. Using loss-of-function mutants *lec-1(ok1597)*, we further found that the total amount of element As(III) was significantly decreased to near background levels in mutants exposed to either As(III) or L-GO concurrently treated with As(III) for 12 h, compared to wild type nematodes (Fig. 8B). Notably, the total amount of element As(III) was increased in a time-dependent manner in wild type nematodes exposed to As(III). The maximum amount of As(III) element was observed in wild type nematodes exposed to As(III) for 24 h. In contrast, the maximum amount of As(III) element in worms exposed to L-GO concurrently with As(III) was detected at 12 h, which was then greatly decreased at 24 h. These findings were confirmed by LA-ICP-MS, as shown in Fig. 8C, suggesting that L-GO not only decreased the bioaccumulation of As(III) but also facilitated its clearance *in vivo*.

To identify the role of LEC-1 in As(III)-induced toxicity, loss-of-function mutants, *lec-1(ok1597)*, were exposed to As(III) or to L-GO concurrently with As(III). The germline apoptosis induced by As(III) was significantly decreased to near background levels in loss-of-function *lec-1(ok1597)* mutants, compared to wild type nematodes (Fig. 8D). The presence of L-GO

1720 | *Environ. Sci.: Nano*, 2018, **5**, 1711–1728

This journal is © The Royal Society of Chemistry 2018

Fig. 6 Autophagy induced by L-GO in *C. elegans*. (A) TEM images of *C. elegans* after exposure to K-medium, L-GO and As(III) and co-exposure to both. The red arrow indicates an autophagosome. (B) qRT-PCR analysis of mRNA levels of autophagy-related genes (*bec-1*, *lgg-1*, *unc-51*, *atg-7*) in control and experimental worms. (C) Average number of germline apoptotic cells in autophagy related gene (*bec-1*, *lgg-1*, and *atg-7*) knockdown in worms. (D and E) Number of germline apoptotic cells induced by K-medium, L-GO, and As(III), and co-exposure to 3-MA (10 μM) and BFA (50 mM). (F) *rpl-43* (*bp399*) mutant and 3-MA, test solution treated *rpl-43* (*bp399*) mutant, and quantitative analysis of the SQST-1::GFP aggregates corresponding to the experimental groups.

This journal is © The Royal Society of Chemistry 2018

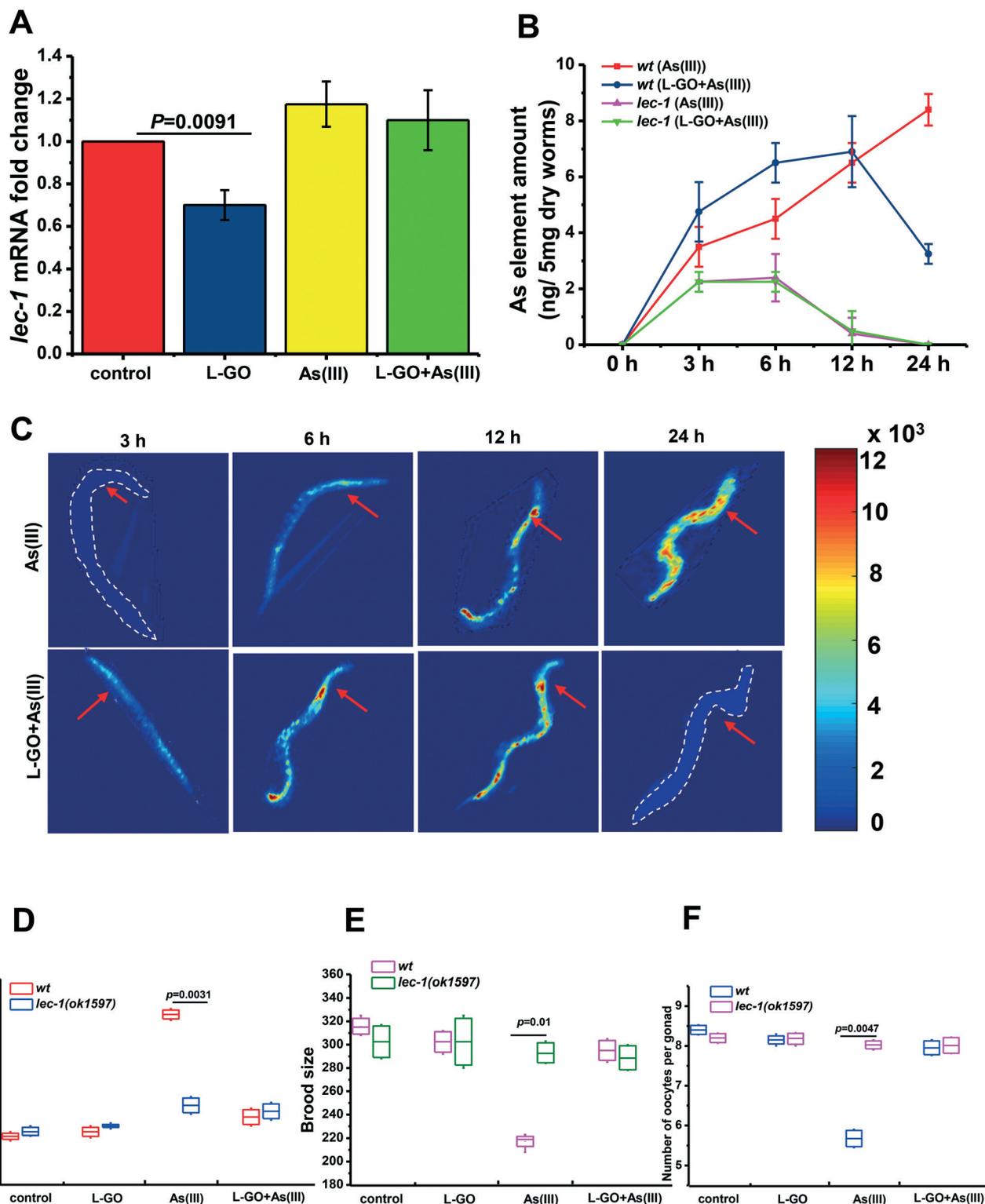*Environ. Sci.: Nano*, 2018, **5**, 1711–1728 | **1721**

Fig. 7 Crucial role of autophagy in *C. elegans* against As(III) toxicity. Effect of (A) *bec-1* gene knockdown and (B) 3-MA on decreased As(III)-induced ROS in L-GO and quantitative analysis of global ROS generated by CM-H$_2$DCFDA.

had a minimal effect on the germline apoptosis induced by As(III) in the loss-of-function *lec-1(ok1597)* mutants. Similarly, the brood size and the number of oocytes per gonad were significantly increased by 36.7% ± 4.21% and 41.0% ± 3.04% in loss-of-function *lec-1(ok1597)* mutants exposed to As(III), respectively; in contrast, there was no significant difference in loss-of-function *lec-1(ok1597)* mutants and wild type nematodes exposed to L-GO concurrently with As(III) (Fig. 8E and F). These data indicated that LEC-1 is essential for As(III) accumulation and toxicity, whereas L-GO alters the

gene expression of *lec-1 in vivo*, which further mediated the bioaccumulation of As(III) and the toxic response.

Discussion

The large theoretical surface area and abundance of oxygen-containing functional groups make GO highly attractive for the removal of heavy metals from contaminated water.[46] The adsorption behavior of GO not only affects the mobility and fate of heavy metals in the environment but also alters their

1722 | *Environ. Sci.: Nano*, 2018, **5**, 1711–1728

This journal is © The Royal Society of Chemistry 2018

Fig. 8 Effect of LEC-1 in attenuating the toxicity of As(III) by L-GO. (A) Relative levels of *lec-1* gene exposure to K-medium, L-GO (10 μg mL^{-1}), and As(III) (10 μM) and co-exposure to L-GO and As(III) for 24 h, detected using qRT-PCR analysis (n = 3). (B) As(III) contents in wild type worms and *lec-1(ok1597)* mutant strain treated with 10 μM As(III) and co-exposed for 3, 6, 12, and 24 h, respectively. As(III) contents were determined using ICP-AFS assay (n = 3). (C) As(III) distribution in wild type worms. As(III) (10 μM) and L-GO co-exposure for 3, 6, 12, and 24 h. (D) Average apoptotic cells, (E) brood size and (F) number of oocytes per gonad after exposure of wild type worms and mutant *lec-1(ok1597)* strain to K-medium, L-GO, As(III) and both (n = 3).

toxic effects on the ecosystem and human health.[47,48] The lateral dimension has no significant effect on a specific surface

area, but the dosage determines the maximum dimension of the material, which plays an essential role in the interaction

This journal is © The Royal Society of Chemistry 2018

Environ. Sci.: Nano, 2018, **5**, 1711–1728 | 1723

with biological systems.[49] GO has a strong tendency to interact with cell surfaces.[50] In the present study, the lateral sizes of GO ranged from 50–1050 nm, as characterized by TEM (Fig. 1). We found that L-GO at a nontoxic concentration (10 $\mu g\ mL^{-1}$) decreased the toxicity of As(III) more efficiently, compared to I-GO and S-GO (Fig. 2A).

The influence of GO on As(III) toxicity may vary depending on the exposure processes in the natural environment. The differential toxicity observed upon changing the sequence of exposure will be helpful to identify the concurrent contribution of GO and As(III) in living organisms. Pretreatment with C60(Nd) nanoparticles (nC60(Nd)) has been shown to dramatically increase chemotherapeutic killing in both normal and drug-resistant cancer cells.[51] Treatment with AgNPs (<0.1 μm) with subsequent exposure to UVA (320–400 nm) showed significantly synergistic antibacterial effects, because of the surface oxidation of AgNPs caused by UVA; in contrast, this phenomenon was not observed in other exposure methods.[52] GO pretreatment did not significantly increase As(III) cytotoxicity in the human hepatoma cell line HepG2; however, when cells were pretreated with As(III) for 12 h, GO significantly increased the cytotoxicity of As(III), indicating that GO could render cells more susceptible to As(III).[20] GO pretreatment significantly increased the cytotoxicity of chemotherapeutic agents to cancer cells, indicating that GO could compromise the cell membrane and cytoskeleton and induce a subsequent cellular priming state making cancer cells more susceptible to chemotherapeutic agents.[53] In our previous in vitro study, we found that GO pretreatment dramatically decreased the toxicity of PCB 52, whereas there was no significant difference in the cytotoxicity with either PCB 52 alone or pretreatment with PCB 52 followed by GO.[21] Using C. elegans as an in vivo model, our data showed that concurrent treatment with GO and As(III) as well as pretreatment with GO followed by As(III) significantly decreased As(III) toxicity; however, pretreatment with As(III) followed by GO treatment exhibited toxic effects similar to As(III) treatment alone (Fig. 2A and 4A and B). We hypothesized that an antagonistic mechanism stimulated by GO might be involved in mediating toxic responses to As(III) in C. elegans. However, the physiochemical interaction between GO and As(III) in living organisms is still unexplored.

Owing to the high surface area of GO, the physical adsorption and catalytic chemical reaction with As(III) is expected to be important to toxic responses in C. elegans. Adsorption of As(III) by GO has been well-documented in various cell-free systems.[11,13] As shown in Fig. 3A and C, As(III) was adsorbed efficiently by L-GO and the maximum absorption capacity for As(III) reached approximately 50%, when the concentration of As(III) was 10 μM. In the human As metabolic pathway, As(V) is converted to As(III), with subsequent methylation to monomethylated and dimethylated arsenicals (MMA and DMA, respectively). Methylated arsenicals, especially MMA, are considered more toxic than As(III) both in animals and human cell lines.[54] GO was reported to assist As(V) entry into cells and to transform As(V) into high toxicity As(III) in wheat,

resulting in enhancement of As(V) phototoxicity.[19] Considering that As(III) can be readily transformed by biological activities and changes in redox potential and pH, the potential transformation of As(III) in the presence or absence of GO was determined in both K-medium and nematodes in the present study. The HPLC-AFS analysis revealed that the As(III) in K-medium, worms, and in excretion metabolites was all in the form of As(III) in the presence of GO (Fig. 3B). Moreover, using centrifugation to harvest the GO-As(III) aggregates in the sediment, we confirmed that the germline apoptosis induced by As(III) was almost totally suppressed by GO compared to As(III) in the supernatant (Fig. 3C). These findings suggested that in addition to adsorption, GO might ameliorate As(III) toxicity via other mechanisms in C. elegans.

Mitochondria as the prime cellular target for As(III) toxicity can actively accumulate As(III).[55] As(III) has a high affinity for thiol (–SH) groups in proteins, causing inactivation of a variety of enzymes including the complexes II and IV of the electron transport chain.[56,57] As the mitochondrial function is highly dependent on the cellular microenvironment and intercellular signals, many of which are lost in vitro, C. elegans represents an excellent in vivo model to investigate the influence of GO on As(III) induced mitochondrial dysfunction. As shown in Fig. 5A–C, GO significantly protected mitochondria from As(III) attack and inhibited ROS generation by As(III). MEV-1, as an integral membrane protein that is a subunit of the mitochondrial respiratory chain complex II, is required for oxidative phosphorylation in C. elegans.[58] We further found that germ cell apoptosis in mev-1(kn 1) mutants exposed to As(III) was significantly higher than that in wild type nematodes at equal concentrations, which was dramatically suppressed by GO (Fig. 5D). These results suggested that GO blocked mitochondrial damage and ROS induction, leading to minimization of As(III) induced toxicity.

Autophagy is an important cellular self-defense process against As(III)-induced toxicity through elimination of misfolded proteins and damaged organelles, especially dysfunctional mitochondria. Exposure to As(III) at low doses for 16 weeks enhanced the intracellular ROS levels in human bronchial epithelial BEAS-2B cells but failed to induce cell transformation because of protection from autophagy in mitochondria turnover.[59,60] As(III) at 100 μM did not induce autophagy gene (lgg-1, atg-18) expression in fusion-deficient nematodes, indicating that autophagy might have a limited role in As(III) toxicity at non-lethal concentrations.[61] No significant intracellular autophagic vacuolization was observed by TEM in nematodes exposed to As(III) at a non-lethal dose of 10 μM in the present study, which was confirmed by autophagy-related gene expression including bec-1, lgg-1, unc-51, and atg-7. GO has been shown to induce autophagic effects in a number of cell lines and acts as a "double-edged sword" in mediating the cellular response to environmental stressors depending on the integrity of the autophagic flux and the molecular mechanisms of autophagy.[62,63] As shown in Fig. 6B and S3,† GO at a non-toxic concentration induced

1724 | Environ. Sci.: Nano, 2018, 5, 1711–1728

This journal is © The Royal Society of Chemistry 2018

autophagic effects in a lateral size-dependent manner. Autophagy related genes were dramatically upregulated in worms exposed to GO with or without As(III), whereas depletion of *bec-1* and *atg-7* function using RNAi partially blocked the protection of GO on As(III) toxicity (Fig. 6C). Autophagy is a dynamic flux and downstream degradation is essential for maintaining its protective role in intracellular homeostasis. Using autophagy inhibitors, like 3-MA and BFA, and the autophagic flux reporter HZ946 rpl-43(bp399); bpIs151(SQST-1::GFP), GO was confirmed to protect nematodes from As(III) through authentic autophagy with valid degradable capacity (Fig. 6D–F). Our data provide clear evidence that GO stimulates a protective barrier and improves the capacity for resistance to As(III)-induced toxicity. A similar protective phenomenon of autophagy was also observed by other researchers with sliver nanoparticles,[64] nanosized paramontroseite VO$_2$,[65] curcumin–temozolomide combination therapy,[66] and dichloroacetate in esophageal squamous carcinoma cells.[67] In general, autophagy is thought to be a nonselective degradation pathway; however, selective substrate adaptor proteins, such as p62 (known as sequestosome 1 (SQSTM1)) have been shown to facilitate the degradation of specific proteins through autophagy.[68] Thus, it is interesting to investigate the influence of GO on specific As(III)-binding proteins, which is the first step in As(III) metabolism *in vivo.*

Galectin-1 (GAL1) is a sugar-binding protein containing six sulfhydryl groups, which serve as high-affinity binding sites for As(III) and are involved in the toxic action of As(III).[69–72] LEC-1 in *C. elegans* is homologous to vertebrate GAL1.[73] Fig. 8A shows that GO significantly suppressed the expression of *lec-1*, and the total As(III) accumulation in nematodes was greatly decreased in the loss-of-function *lec-1(ok1597)* mutants (Fig. 8B). Notably, although GO facilitated the As(III) accumulation in wild type nematodes in the first 12 h, the total amount of As(III) was greatly decreased in worms with concurrent exposure to GO for 24 h. LA-ICP-MS is a powerful mapping technique to generate quantitative images of detailed regionally specific element distributions and has been successfully applied in *C. elegans.*[74,75] Fig. 8C further provides real time *in vivo* evidence of As(III) accumulation in wild type nematodes concurrently exposed to GO and showed that GO facilitated the uptake and excretion of As(III). It has been proposed that GO influences the As(III) uptake *via* co-transportation.[19] We speculated that the adsorption of As(III) on GO might ease the accumulation of As(III); however, suppression of LEC-1 by GO eventually facilitated As(III) clearance *in vivo.* The expression of autophagy related genes such as *bec-1* and *lgg-1* was upregulated in the loss-of-function mutants *lec-1(ok1597)* compared to the wild-type worms (Fig. S4†); however, information on the role of LEC-1 in autophagy is very scarce. Limited investigation on hepatocellular carcinoma (HCC) chemotherapy suggested that GAL-1 decreased the efficacy of cisplatin treatment through autophagy induction.[76]

Conclusion

Our results highlight the protective mechanisms of GO in decreasing As(III) toxicity. In addition to adsorption, two main aspects were involved in this antagonistic process: (a) GO activated protective autophagy to block oxidative stress induced by As(III). (b) GO accelerated the excretion of As(III) by downregulating the expression of an As(III) binding protein (LEC-1). Given the widespread use of GO as an adsorbent to remove As, it is highly important to study the interaction between GO and As and the effects of GO on As-induced toxicity in the ecosystem and in human beings.

Authors' contributions

H. D. and A. X. conceived and designed the experiments. J. J. W. executed qRT-PCR and toxicity assays, and Y. L. and Y. G. N. wrote the manuscript. All the authors discussed the results and commented on the manuscript.

Conflicts of interest

The authors declare that they have no competing interests.

Acknowledgements

References

1 R. N. Ratnaike, Acute and chronic arsenic toxicity, *Postgrad. Med. J.*, 2003, **79**, 391–396.

2 K. H. Morales, L. Ryan, T. L. Kuo, M. M. Wu and C. J. Chen, Risk of internal cancers from arsenic in drinking water, *Environ. Health Perspect.*, 2000, **108**, 655.

3 S. Kapaj and H. Peterson, Human health effects from chronic arsenic poisoning–a review, *J. Environ. Sci. Health, Part A: Toxic/Hazard. Subst. Environ. Eng.*, 2006, **41**, 2399.

4 R. Singh, S. Singh, P. Parihar, V. P. Singh and S. M. Prasad, Arsenic contamination, consequences and remediation techniques: a review, *Ecotoxicol. Environ. Saf.*, 2015, **112**, 247.

5 A. Sarkar and B. Paul, The global menace of arsenic and its conventional remediation - A critical review, *Chemosphere*, 2016, **158**, 37.

6 L. Ji, W. Chen, Z. Xu, S. Zheng and D. Zhu, Graphene nanosheets and graphite oxide as promising adsorbents for

This journal is © The Royal Society of Chemistry 2018

Environ. Sci.: Nano, 2018, **5**, 1711–1728 | 1725

removal of organic contaminants from aqueous solution, *J. Environ. Qual.*, 2013, **42**, 191.

7 A. K. Geim, Science, Graphene: Status and Prospects, *Science*, 2009, **324**, 1530–1534.

8 L. Zhang, J. Xia, Q. Zhao, L. Liu and Z. Zhang, Functional Graphene Oxide as a Nanocarrier for Controlled Loading and Targeted Delivery of Mixed Anticancer Drugs, *Small*, 2010, **6**, 537–544.

9 G. Zhao, J. Li, X. Ren, C. Chen and X. Wang, Few-layered graphene oxide nanosheets as superior sorbents for heavy metal ion pollution management, *Environ. Sci. Technol.*, 2011, **45**, 10454–10462.

10 H. Yan, H. Wu, K. Li, Y. Wang, X. Tao, H. Yang, A. Li and R. Cheng, Influence of the Surface Structure of Graphene Oxide on the Adsorption of Aromatic Organic Compounds from Water, *ACS Appl. Mater. Interfaces*, 2015, **7**, 6690.

11 V. Chandra, J. Park, Y. Chun, J. W. Lee, I. C. Hwang and K. S. Kim, Water-Dispersible Magnetite-Reduced Graphene Oxide Composites for Arsenic Removal, *ACS Nano*, 2010, **4**, 3979.

12 X. Luo, C. Wang, L. Wang, F. Deng and S. Luo, X. Tu and C. Au, Nanocomposites of graphene oxide-hydrated zirconium oxide for simultaneous removal of As(III) and As(v) from water, *Chem. Eng. J.*, 2013, **220**, 98–106.

13 S. Kumar, R. R. Nair, P. B. Pillai, S. N. Gupta, M. A. Iyengar and A. K. Sood, Graphene oxide-MnFe2O4 magnetic nanohybrids for efficient removal of lead and arsenic from water, *ACS Appl. Mater. Interfaces*, 2014, **6**, 17426.

14 Z. Kai, V. Dwivedi, C. Chi and J. Wu, Graphene oxide/ferric hydroxide composites for efficient arsenate removal from drinking water, *J. Hazard. Mater.*, 2010, **182**, 162.

15 J. H. Zhu, R. Sadu, S. Y. Wei, D. H. Chen, N. Haldolaarachchige, Z. P. Luo, J. A. Gomes, D. P. Young and Z. H. Guo, Magnetic Graphene Nanoplatelet Composites toward Arsenic Removal, *ECS J. Solid State Sci. Technol.*, 2012, **1**, M1–M5.

16 A. Salvati, Biomolecular coronas provide the biological identity of nanosized materials, *Nat. Nanotechnol.*, 2012, **7**, 779–786.

17 A. Lesniak, A. Salvati, M. J. Santosmartinez, M. W. Radomski, K. A. Dawson and C. Åberg, Nanoparticle Adhesion to the Cell Membrane and Its Effect on Nanoparticle Uptake Efficiency, *J. Am. Chem. Soc.*, 2013, **135**, 1438.

18 W. Fengjuan, Y. Lu, M. P. Monopoli, S. Peter, M. Eugene, S. Anna and K. A. Dawson, The biomolecular corona is retained during nanoparticle uptake and protects the cells from the damage induced by cationic nanoparticles until degraded in the lysosomes, *Nanomedicine*, 2013, **9**, 1159–1168.

19 X. Hu, J. Kang, K. Lu, R. Zhou, L. Mu and Q. Zhou, Graphene oxide amplifies the phytotoxicity of arsenic in wheat, *Sci. Rep.*, 2014, **4**, 6122.

20 L. Su, J. Wei, W. Bing, Y. Jing, H. Yu, X. X. Zhang, C. Torres-Duarte and G. N. Cherr, Low levels of graphene and graphene oxide inhibit cellular xenobiotic defense system mediated by efflux transporters, *Nanotoxicology*, 2016, **10**, 597.

21 Y. Liu, X. Wang, J. Wang, Y. Nie, H. Du, H. Dai, J. Wang, M. Wang, S. Chen and T. K. Hei, Graphene oxide attenuates the cytotoxicity and mutagenicity of PCB 52 via activation of genuine autophagy, *Environ. Sci. Technol.*, 2016, **50**, 777–779.

22 W. A. Boyd, M. V. Smith and J. H. Freedman, *Caenorhabditis elegans as a Model in Developmental Toxicology*, Humana Press, 2012.

23 P. L. Williams and D. B. Dusenbery, Aquatic toxicity testing using the nematode, Caenorhabditis elegans, *Environ. Toxicol. Chem.*, 2010, **9**, 1285–1290.

24 M. C. K. Leung, P. L. Williams, B. Alexandre, A. Catherine, K. J. Helmcke, A. Michael and J. N. Meyer, Caenorhabditis elegans: An Emerging Model in Biomedical and Environmental Toxicology, *Toxicol. Sci.*, 2008, **106**, 5.

25 E. Zanni, B. G. De, M. P. Bracciale, A. Broggi, M. L. Santarelli, M. S. Sarto, C. Palleschi and D. Uccelletti, Graphite nanoplatelets and Caenorhabditis elegans: insights from an in vivo model, *Nano Lett.*, 2012, **12**, 2740.

26 D. Barsyte, D. A. Lovejoy and G. J. Lithgow, Longevity and heavy metal resistance in daf-2 and age-1 long-lived mutants of Caenorhabditis elegans, *FASEB J.*, 2001, **15**, 627–634.

27 S. Shankar, U. Shanker and Shikha, Arsenic contamination of groundwater: a review of sources, prevalence, health risks, and strategies for mitigation, *Sci. World J.*, 2014, **2014**, 304524.

28 W. S. Hummers and R. E. Offeman, Preparation of Graphitic Oxide, *J. Am. Chem. Soc.*, 1958, **80**, 1339–1339.

29 S. Brenner, The genetics of Caenorhabditis elegans, *Genetics*, 1974, 77, 71.

30 B. Lant and W. B. Derry, Fluorescent visualization of germline apoptosis in living Caenorhabditis elegans, *Cold Spring Harb. Protoc.*, 2014, **2014**, 420–427.

31 S. C. Swain, K. Keusekotten, R. Baumeister and S. R. Sturzenbaum, C-elegans metallothioneins: New insights into the phenotypic effects of cadmium toxicosis, *J. Mol. Biol.*, 2004, **341**, 951–959.

32 S. G. Brinkhaus, J. Bornhorst, S. Chakraborty, C. A. Wehe, R. Niehaus, O. Reifschneider, M. Aschner and U. Karst, Elemental bioimaging of manganese uptake in C-elegans, *Metallomics*, 2014, **6**, 617–621.

33 M. Li, Z. Luo, Y. Yan, Z. Wang, Q. Chi, C. Yan and B. Xing, Arsenate Accumulation, Distribution, and Toxicity Associated with Titanium Dioxide Nanoparticles in Daphnia magna, *Environ. Sci. Technol.*, 2016, **50**, 9636–9643.

34 R. S. Kamath, A. G. Fraser, Y. Dong, G. Poulin, R. Durbin, M. Gotta, A. Kanapin, N. Le Bot, S. Moreno, M. Sohrmann, D. P. Welchman, P. Zipperlen and J. Ahringer, Systematic functional analysis of the Caenorhabditis elegans genome using RNAi, *Nature*, 2003, **421**, 231–237.

35 W. B. Iser, D. Kim, E. Bachman and C. Wolkow, Examination of the requirement for ucp-4, a putative homolog of mammalian uncoupling proteins, for stress tolerance and longevity in C-elegans, *Mech. Ageing Dev.*, 2005, **126**, 1090–1096.

1726 | *Environ. Sci.: Nano*, 2018, **5**, 1711–1728

This journal is © The Royal Society of Chemistry 2018

36 L. M. Sun, Z. Q. Lin, K. Liao, Z. G. Xi and D. Y. Wang, Adverse effects of coal combustion related fine particulate matter (PM2.5) on nematode Caenorhabditis elegans, *Sci. Total Environ.*, 2015, **512**, 251–260.

37 H. A. Becerril, J. Mao, Z. Liu, R. M. Stoltenberg, Z. Bao and Y. Chen, Evaluation of solution-processed reduced graphene oxide films as transparent conductors, *ACS Nano*, 2008, **2**, 463.

38 P. Khanra, T. Kuila, N. H. Kim, S. H. Bae, D. S. Yu and J. H. Lee, Simultaneous bio-functionalization and reduction of graphene oxide by baker's yeast, *Chem. Eng. J.*, 2012, **183**, 526–533.

39 N. Senoo-Matsuda, P. S. Hartman, A. Akatsuka, S. Yoshimura and N. Ishii, A complex II defect affects mitochondrial structure, leading to ced-3- and ced-4-dependent apoptosis and aging, *J. Biol. Chem.*, 2003, **278**, 22031–22036.

40 N. Pallet, N. Bouvier, C. Legendre, J. Gilleron, P. Codogno, P. Beaune, E. Thervet and D. Anglicheau, Autophagy protects renal tubular cells against cyclosporine toxicity, *Autophagy*, 2008, **4**, 783–791.

41 E. S. Hars, H. Y. Qi, A. G. Ryazanov, S. K. Jin, L. Cai, C. C. Hu and L. F. Liu, Autophagy regulates ageing in C-elegans, *Autophagy*, 2007, **3**, 93–95.

42 Y. Stroikin, H. Dalen, S. Loof and A. Terman, Inhibition of autophagy with 3-methyladenine results in impaired turnover of lysosomes and accumulation of lipofuscin-like material, *Eur. J. Cell Biol.*, 2004, **83**, 583–590.

43 P. O. Seglen and P. B. Gordon, 3-Methyladenine - Specific Inhibitor of Autophagic Lysosomal Protein-Degradation in Isolated Rat Hepatocytes, *Proc. Natl. Acad. Sci. U. S. A.*, 1982, **79**, 1889–1892.

44 D. C. Rubinsztein, A. M. Cuervo, B. Ravikumar, S. Sarkar, V. Korolchuk, S. Kaushik and D. J. Klionsky, In search of an autophagomometer, *Autophagy*, 2009, **5**, 585–589.

45 Y. F. Zhou, Q. Wang, B. Song, S. C. Wu, Y. Y. Su, H. M. Zhang and Y. He, A real-time documentation and mechanistic investigation of quantum dots-induced autophagy in live Caenorhabditis elegans, *Biomaterials*, 2015, **72**, 38–48.

46 G. Z. Kyzas, E. A. Deliyanni and K. A. Matis, Graphene oxide and its application as an adsorbent for wastewater treatment, *J. Chem. Technol. Biotechnol.*, 2014, **89**, 196–205.

47 J. Zhao, Z. Wang, J. C. White and B. Xing, Graphene in the Aquatic Environment: Adsorption, Dispersion, Toxicity and Transformation, *Environ. Sci. Technol.*, 2014, **48**, 9995–10009.

48 R. R. Rosenfeldt, F. Seitz, J. P. Zubrod, A. Feckler, T. Merkel, S. Lüderwald, R. Bundschuh, R. Schulz and M. Bundschuh, Does the presence of titanium dioxide nanoparticles reduce copper toxicity? A factorial approach with the benthic amphipod Gammarus fossarum, *Aquat. Toxicol.*, 2015, **165**, 154.

49 H. Yue, W. Wei, Z. Yue, B. Wang, N. Luo, Y. Gao, D. Ma, G. Ma and Z. Su, The role of the lateral dimension of graphene oxide in the regulation of cellular responses, *Biomaterials*, 2012, **33**, 4013–4021.

50 X. Zhang, W. Hu, J. Li, L. Tao and Y. Wei, A comparative study of cellular uptake and cytotoxicity of multi-walled carbon nanotubes, graphene oxide, and nanodiamond, *Toxicol. Res.*, 2012, **1**, 62–68.

51 P. Wei, L. Zhang, Y. Lu, N. Man and L. Wen, C60(Nd) nanoparticles enhance chemotherapeutic susceptibility of cancer cells by modulation of autophagy, *Nanotechnology*, 2010, **21**, 495101.

52 X. Zhao, T. Toyooka and Y. Ibuki, Synergistic bactericidal effect by combined exposure to Ag nanoparticles and UVA, *Sci. Total Environ.*, 2013, **458–460**, 54–62.

53 J. Zhu, M. Xu, M. Gao, Z. Zhang, Y. Xu, T. Xia and S. Liu, Graphene Oxide-Induced Perturbation to Plasma Membrane and Cytoskeletal Meshwork Sensitize Cancer Cells to Chemotherapeutic Agents, *ACS Nano*, 2017, **11**, 2637–2651.

54 X. C. Le, X. Lu, M. Ma, W. R. Cullen, H. V. Aposhian and B. Zheng, Speciation of Key Arsenic Metabolic Intermediates in Human Urine, *Anal. Chem.*, 2000, **72**, 5172.

55 Z. Y. Shen, J. Shen, W. J. Cai, C. Hong and M. H. Zheng, The alteration of mitochondria is an early event of arsenic trioxide induced apoptosis in esophageal carcinoma cells, *Int. J. Mol. Med.*, 2000, **5**, 155.

56 J. C. Saha, A. K. Dikshit, M. Bandyopadhyay and K. C. Saha, A Review of Arsenic Poisoning and its Effects on Human Health, *Crit. Rev. Environ. Sci. Technol.*, 1999, **29**, 281–313.

57 L. K. Nutt, V. Gogvadze, W. Uthaisang, B. Mirnikjoo, D. J. Mcconkey and S. Orrenius, Indirect effects of Bax and Bak initiate the mitochondrial alterations that lead to cytochrome c release during arsenic trioxide-induced apoptosis, *Cancer Biol. Ther.*, 2005, **4**, 459.

58 N. Senoomatsuda, P. S. Hartman, A. Akatsuka, S. Yoshimura and N. Ishii, A complex II defect affects mitochondrial structure, leading to ced-3- and ced-4-dependent apoptosis and aging, *J. Biol. Chem.*, 2003, **278**, 22031.

59 T. Zhang, Y. Qi, M. Liao, M. Xu, K. A. Bower, J. A. Frank, H. M. Shen, J. Luo, X. Shi and G. Chen, Autophagy Is a Cell Self-Protective Mechanism Against Arsenic-Induced Cell Transformation, *Toxicol. Sci.*, 2012, **130**, 298.

60 Y. Qi, M. Zhang, H. Li, J. A. Frank, L. Dai, H. Liu, Z. Zhang, C. Wang and G. Chen, Autophagy Inhibition by Sustained Overproduction of IL6 Contributes to Arsenic Carcinogenesis, *Cancer Res.*, 2014, **74**, 3740.

61 A. L. Luz, T. R. Godebo, L. L. Smith, T. C. Leuthner, L. L. Maurer and J. N. Meyer, Deficiencies in mitochondrial dynamics sensitize Caenorhabditis elegans to arsenite and other mitochondrial toxicants by reducing mitochondrial adaptability, *Toxicology*, 2017, **387**, 81.

62 G. Y. Chen, H. J. Yang, C. H. Lu, Y. C. Chao, S. M. Hwang, C. L. Chen, K. W. Lo, L. Y. Sung, W. Y. Luo and H. Y. Tuan, Simultaneous induction of autophagy and toll-like receptor signaling pathways by graphene oxide, *Biomaterials*, 2012, **33**, 6559.

63 R. Scherz-Shouval and Z. Elazar, ROS, mitochondria and the regulation of autophagy, *Trends Cell Biol.*, 2007, **17**, 422–427.

64 J. Lin, Z. Huang, H. Wu, W. Zhou, P. Jin, P. Wei, Y. Zhang, F. Zheng, J. Zhang and J. Xu, Inhibition of autophagy enhances the anticancer activity of silver nanoparticles, *Autophagy*, 2014, **10**, 2006–2020.

This journal is © The Royal Society of Chemistry 2018

Environ. Sci.: Nano, 2018, **5**, 1711–1728 | 1727

65 W. Zhou, Y. Miao, Y. Zhang, L. Liu, J. Lin, J. Y. Yang, Y. Xie and L. Wen, Induction of cyto-protective autophagy by para-montroseite VO2 nanocrystals, *Nanotechnology*, 2013, **24**, 165102.

66 A. Zanottofilho, E. Braganhol, K. Klafke, S. R. Terra, F. J. Paludo, M. Morrone, I. J. Bristot, A. M. Battastini, C. M. Forcelini and A. J. Bishop, Autophagy inhibition improves the efficacy of curcumin/temozolomide combination therapy in glioblastomas, *Cancer Lett.*, 2015, **358**, 220–231.

67 H. Y. Jia, H. N. Wang, F. Y. Xia, Y. Sun, H. L. Liu, L. L. Yan, S. S. Li, D. C. Jiang and M. M. Xu, Dichloroacetate induces protective autophagy in esophageal squamous carcinoma cells, *Oncol. Lett.*, 2017, **14**, 2765.

68 G. Bjørkøy, T. Lamark, A. Brech, H. Outzen, M. Perander, A. Overvatn, H. Stenmark and T. Johansen, *et al.* p62/SQSTM1 forms protein aggregates degraded by autophagy and has a protective effect on huntingtin-induced cell death, *J. Cell Biol.*, 2005, **171**, 603–614.

69 S. H. Barondes, D. N. Cooper, M. A. Gitt and H. Leffler, Galectins. Structure and function of a large family of animal lectins, *J. Biol. Chem.*, 1994, **269**, 20807–20810.

70 D. I. Liao, G. Kapadia, H. Ahmed, G. R. Vasta and O. Herzberg, Structure of S-lectin, a developmentally regulated vertebrate beta-galactoside-binding protein, *Proc. Natl. Acad. Sci. U. S. A.*, 1994, **91**, 1428–1432.

71 Y. Y. Chang, M. C. Chiang, T. C. Kuo, L. L. Chi, Y. H. Kao and R. N. Huang, The down-regulation of galectin-1 expression is a specific biomarker of arsenic toxicity, *Toxicol. Lett.*, 2011, **205**, 38–46.

72 C. H. Lin, C. F. Huang, W. Y. Chen, Y. Y. Chang, W. H. Ding, M. S. Lin and S. H, Wu and R. N. Huang, Characterization of the interaction of galectin-1 with sodium arsenite, *Chem. Res. Toxicol.*, 2006, **19**, 469–474.

73 J. Hirabayashi, M. Satoh and K. Kasai, Evidence that Caenorhabditis elegans 32-kDa beta-galactoside-binding protein is homologous to vertebrate beta-galactoside-binding lectins. cDNA cloning and deduced amino acid sequence, *J. Biol. Chem.*, 1992, **267**, 15485–15490.

74 M. T. Li, Z. X. Luo, Y. M. Yan, Z. H. Wang, Q. Q. Chi, C. Z. Yan and B. S. Xing, Arsenate Accumulation, Distribution, and Toxicity Associated with Titanium Dioxide Nanoparticles in Daphnia magna, *Environ. Sci. Technol.*, 2016, **50**, 9636–9643.

75 J. S. Becker, A. Matusch and B. Wu, Bioimaging mass spectrometry of trace elements - recent advance and applications of LA-ICP-MS: A review, *Anal. Chim. Acta*, 2014, **835**, 1–18.

76 Y. C. Su, G. V. Davuluri, C. H. Chen, D. C. Shiau, C. C. Chen, C. L. Chen, Y. S. Lin and C. P. Chang, Galectin-1-Induced Autophagy Facilitates Cisplatin Resistance of Hepatocellular Carcinoma, *PLoS One*, 2016, **11**, e0148408.